J Therm Anal Calorim (2016) 126:617–625
DOI 10.1007/s10973-016-5522-7

Second law analysis of a nanofluid-based solar collector using experimental data

Saleh Salavati Meibodi[1] · Ali Kianifar[1] · Omid Mahian[2] · Somchai Wongwises[3]

Received: 11 April 2016 / Accepted: 1 May 2016 / Published online: 23 May 2016

Abstract The present study deals with the entropy generation analysis of a flat-plate solar collector using SiO_2/ethylene glycol–water nanofluids. For this purpose, available experimental data on the performance of a flat-plate solar collector are exploited for estimating the entropy generation in the system. Ethylene glycol–water (EG–water) and EG–water-based nanofluids having three different nanoparticle volume fractions including 0.5, 0.75, and 1 % are considered as the working fluids. The results are presented in terms of exergy efficiency, entropy generation parameter, and Bejan number for three different mass flow rates and various solar radiation intensities. It is found that when nanofluid concentration increases from 0 to 1 %, exergy efficiency enhances up to 62.7 % for a mass flow rate of 1 L min^{-1}, whereas the corresponding increases in mass flow rates of 1.75 and 2.5 L min^{-1} are 45.2 and 39.7 %, respectively. The results also elucidate that entropy generation parameter, which is a function of entropy generation, ambient temperature, and solar radiation, reduces with increasing the nanofluid concentration.

Keywords Nanofluid · Solar collector · Entropy generation · Experimental data

✉ Ali Kianifar
a-kiani@um.ac.ir

[1] Department of Mechanical Engineering, Ferdowsi University of Mashhad, Mashhad, Iran

[2] Young Researchers and Elite Club, Mashhad Branch, Islamic Azad University, Mashhad, Iran

[3] Fluid Mechanics, Thermal Engineering and Multiphase Flow Research Laboratory (FUTURE), Department of Mechanical Engineering, Faculty of Engineering, King Mongkut's University of Technology Thonburi (KMUTT), Bangmod, Bangkok 10140, Thailand

Introduction

Nowadays, "Nanofluid" has converted to a well-known term in the dictionary of thermal engineering. Many studies have been carried out to determine the thermophysical properties of various nanofluids (for example, see Refs. [1–8]) since the design accuracy of thermal systems depends strongly on the properties of working fluid. In parallel, researchers have developed the exploitation of nanofluids in various engineering systems such as automotive sector [9], micro-/minichannels [10], heat exchangers [11–14], and solar energy devices [15, 16].

One of the applications of nanofluids is in flat-plate solar collectors as the most common solar systems. The literature includes a considerable number of studies on the thermal efficiency of solar collectors where a nanofluid is working fluid. However, fewer studies are performed on the exergy efficiency and entropy generation of solar collectors using nanofluids, whereas exergy analysis of a thermal system is vital to recognize the energy loss factors. Here, a brief review is presented on the previous studies on the exergy and entropy generation analysis of flat-plate solar collectors. Alim et al. [17] investigated the exergy efficiency of a flat-plate solar collector using four different nanofluids including ZnO/water, CeO_2/water, NiO, and CoO/water nanofluids theoretically. Their results showed a linear increase in exergy efficiency with the volume fraction of nanoparticles and the mass flow rate of nanofluids. They indicated that CeO_2 and ZnO nanoparticles show the highest and smallest exergy efficiencies, respectively. Faizal et al. [18] investigated the exergy efficiency of a flat-plate solar collector using SiO_2/water nanofluids with volume fractions of 0.2 and 0.4 % where the size of nanoparticles was 15 nm. They found that exergy efficiency increased with increasing the volume fraction,

whereas the entropy generation decreased by particle loading. Said et al. [19] examined the exergy efficiency and entropy generation for a solar collector with four different nanoparticles including single-wall carbon nanotubes (SWCNTs), TiO_2, SiO_2, and Al_2O_3 nanoparticles dispersed in water as the base fluid analytically. They found that SWCNTs nanofluids provided the minimum entropy generation in the system.

Mahian et al. [20] theoretically evaluated the effects of uncertainties in thermophysical properties on entropy generation of Al_2O_3/water nanofluids in a solar collector (flat-plate type) where the flow was turbulent. The results were presented in terms of constant mass flow rates and for different values of nanoparticle size (ranging from 25 to 100 nm) by considering the tube roughness. They found that different models that were exploited to calculate the properties had no a significant effect on the entropy generation, independent of nanofluid concentration, and mass flow rate. The tube roughness effects on the entropy generation were pronounced at high mass flow rates. It was also elucidated that the reduction in entropy generation in the solar collector occurs by nanoparticle loading. Later, Mahian et al. [21] assessed the entropy generation due to the flow of boehmite alumina/EG–water nanofluids with volume concentrations up to 4 % in a flat-plate solar collector where nanoparticles had four different shapes including platelets, cylinders, blades, and bricks. Moreover, the entropy generation was examined for collector tubes made of two different materials, i.e., copper and steel. The results unveiled that when the collector tubes are fabricated of copper tubes, using nanofluids containing brick-shaped nanoparticles with concentrations of 2 % concentration leads to entropy generation minimization in the system. However, for steel-based solar collector, 4 % blade-shaped nanoparticles are needed to minimize the entropy generation. It was also found that the entropy generation for copper-based collector is, on average, 11–18 % (depends on the mass flow rate) less than steel-based collector. Mahian et al., in separate studies, investigated the effects of nanofluid pH [22]using four different nanofluids including Cu/water, Al_2O_3/water, TiO_2/water, and SiO_2/water [23] on the entropy generation of a solar collector. Said et al. [24] reported the exergy efficiency of a flat-plate solar collector using Al_2O_3/water nanofluids with volume fractions of 0.1 and 0.3 % and mass flow rates ranging from 0.5 to 1.5 kg min^{-1} where the nanoparticles size was 13 nm. It was found that the exergy efficiency ameliorated by about 20 % when the mass flow rate was 1 kg min^{-1} and the volume fraction was 0.1 %. In a similar study, Said et al. [25] examined exergy efficiency of a flat-plate solar collector using SWCNTs/water nanofluids where the properties of nanofluid samples were measured experimentally. Shojaeizadeh et al. [26] analyzed the exergy efficiency of a flat-plate solar collector using Al_2O_3/water nanofluids. In the study, they found the optimum conditions in which the exergy efficiency was maximized. Shojaeizadeh and Veysi [27] considered the flow of Al_2O_3/water nanofluids in a flat-plate solar collector and developed a correlation for the optimum exergy efficiency. They indicated that the values of mass flow rate, nanoparticle volume fraction, and inlet temperature in which the exergy efficiency was optimized will be reduced with the environmental parameter that was defined as the ratio of ambient temperature to solar radiation.

The present paper aims to analyze the second law of thermodynamics for a flat-plate solar collector using SiO_2 nanoparticles with a diameter of 40 nm suspended in a mixture of EG and water (50:50 vol%). Experimental data reported in our previous work [28] are used in this study. For the analysis, the effects of concentration and mass flow rate of nanofluids on the exergy efficiency and a dimensionless entropy generation number (N_s), which is defined as a function of dimensional entropy generation, ambient temperature, and solar radiation, are evaluated. It should be noted that based on the best knowledge of the authors, it is the first time that the dimensionless entropy generation number is exploited to investigate the nanofluid-based solar collectors.

Experimental

As the details of experiments are available in Ref. [28], here just a brief description of nanofluid preparation and experimental setup is presented.

Nanofluid preparation

Nanofluids have been prepared in three different volume fractions including 0.5, 0.75, and 1 %. For this purpose,

Fig. 1 Prepared samples of SiO_2/EG–water nanofluids

specified amounts of SiO_2 nanoparticles having a diameter of 40 nm were dispersed in the mixture of EG and water (50:50 vol%) by the aid of a mixer and an ultrasonic processor. Specified amount of nanoparticles (depends on the volume fraction) was gradually added to the base fluid, and at the same time, the suspension was stirred for about 30 min. After mixing, the suspension is sonicated with an ultrasonic processor for about 2 h. No surfactant was used in the preparation process. It was observed that the nanofluids have high stability even after months, and no sedimentation was seen with naked eyes. Figure 1 displays a photograph of nanofluid samples.

in the collector with three different mass flow rates including 1, 1.75, and 2.5 L min^{-1}. Experiments have been performed from 10:30 a.m. to 2:30 p.m. The accuracy of thermocouples, pyranometer, timer, and the vessel that is used for measuring the mass flow rate is 0.1 °C, 0.1 W m^{-2}, 0.01 s, and 1 mL, respectively.

Data analysis

The entropy generation rate in the solar collector is obtained by the following relation [20–23]:

$$\dot{S}_{\text{gen}} = \underbrace{\eta_o G_t A_c \left(\frac{1}{T_p} - \frac{1}{T_S}\right) + \dot{m} C_{P,nf} \left(\ln\left(\frac{T_{out}}{T_{in}}\right) - \frac{(T_{out} - T_{in})}{T_P}\right) + U_L A_c \left(1 - \frac{T_a}{T_p}\right)\left(\frac{T_p}{T_a} - 1\right)}_{\dot{S}_{gen})_H} + \underbrace{\frac{\dot{m}\Delta P}{\rho_{nf}} \frac{\ln\left(\frac{T_{out}}{T_a}\right)}{(T_{out} - T_{in})}}_{\dot{S}_{gen})_F} \tag{1}$$

Experiments on solar collector

Figure 2 depicts a schematic of the experimental setup, and Fig. 3 illustrates a photograph of the flat-plate solar collector. Also, the specifications of the solar collector are summarized in Table 1. In each cycle of nanofluid circulation, the fluid is heated up in the solar collector and returns to the tank for the cooling process. Nanofluids flow

where η_o is the optical efficiency and is equal to 0.84, G_t is the solar radiation, A_c is the solar collector surface area, $\dot{m}$ is the mass flow rate, C_p is the heat capacity, ρ_{nf} is the density of nanofluid, and $\Delta P$is the pressure drop. Also, T_S is the apparent sun temperature and approximately equals to 4350 K, i.e., 75 % of blackbody temperature of the sun [29, 30], T_p is the absorber plate temperature, and it is calculated by:

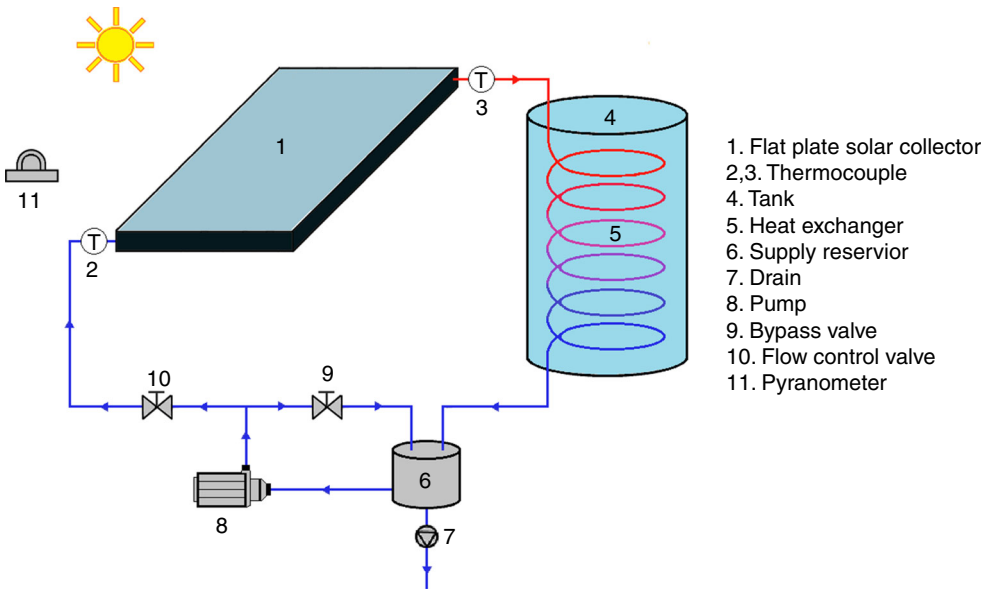

Fig. 2 A schematic of the experimental setup

Fig. 3 A photograph of the solar collector

Table 1 Specifications of the solar collector

External dimensions	925 × 1925 × 93 mm
Gross area	1.781 m^2
Absorber area	1.591 m^2
Absorber material	Black-painted aluminum
Tube material	Aluminum
Diameter of absorber tubes	16 mm
Diameter of header tubes	29 mm
Glass material	Normal glass
Thickness of glass	4 mm
Thermal insulation material	Glass wool K = 0.04 Wm^{-1} k^{-1}
Thickness of thermal insulation	50 mm
Mass	32.5 kg
Casing material	Electrostatic painted aluminum case
Sealing material	EPDM and silicon and aluminum frame
Nanofluid volume in the cycle	3.5 L

$$T_p = T_{in} + \frac{\dot{m}C_{p,nf}(T_{out} - T_{in})}{A_c F_R U_L}(1 - F_R) \quad (2)$$

in which inlet and outlet temperatures are replaced by measured data. Two parameters including F_R (heat removal factor) and $F_R U_L$ (removed energy parameter) are obtained based on the experiments in our former work [28].

The pressure drop in the system is estimated by the following relation [20–23]:

$$\Delta P = P_1 - P_2 = \rho_{nf}\, g\, (L_r \mathrm{Sin}\beta + h_L) \quad (3)$$

where β is the collector slope and L_r is length of riser. The total head loss, h_L, is obtained by:

$$h_L = \frac{8\dot{m}_r^2}{(\rho_{nf})^2 g\pi^2 D_i^4}\left(f\frac{L_r}{D_i} + \sum K_L\right) \quad (4)$$

where $\dot{m}_r$ is the corresponding mass flow rate of one riser, D_i is the inner diameter of riser, K_L is loss coefficient(for laminar flow when flow enters the pipe is 0.5 and when the flow exits the pipe is 2), and friction factor (f) equals $\frac{64}{Re}$ since the flow regime is laminar in the present work. The density and specific heat capacity of nanofluids are calculated by [31]:

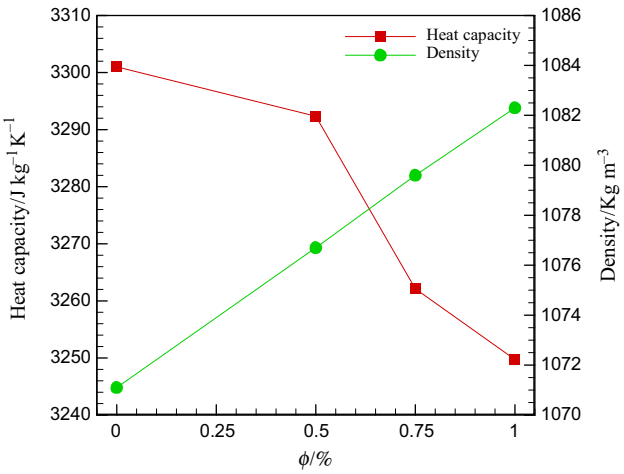

Fig. 4 Variations of heat capacity and density with nanoparticle volume fraction

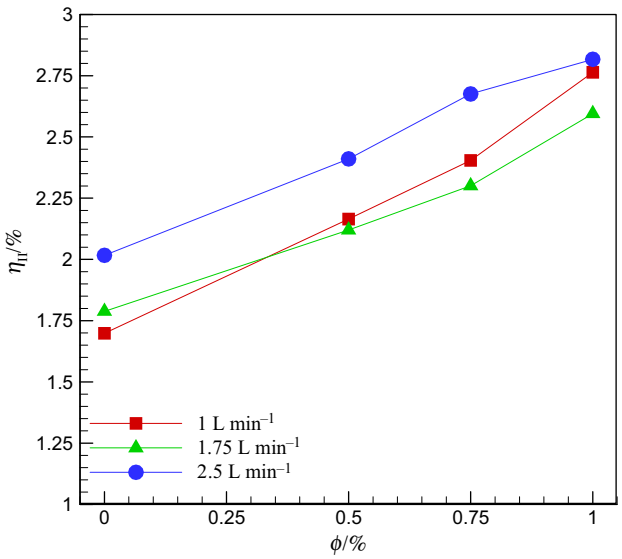

Fig. 5 Variations of exergy efficiency with volume fraction for different mass flow rates

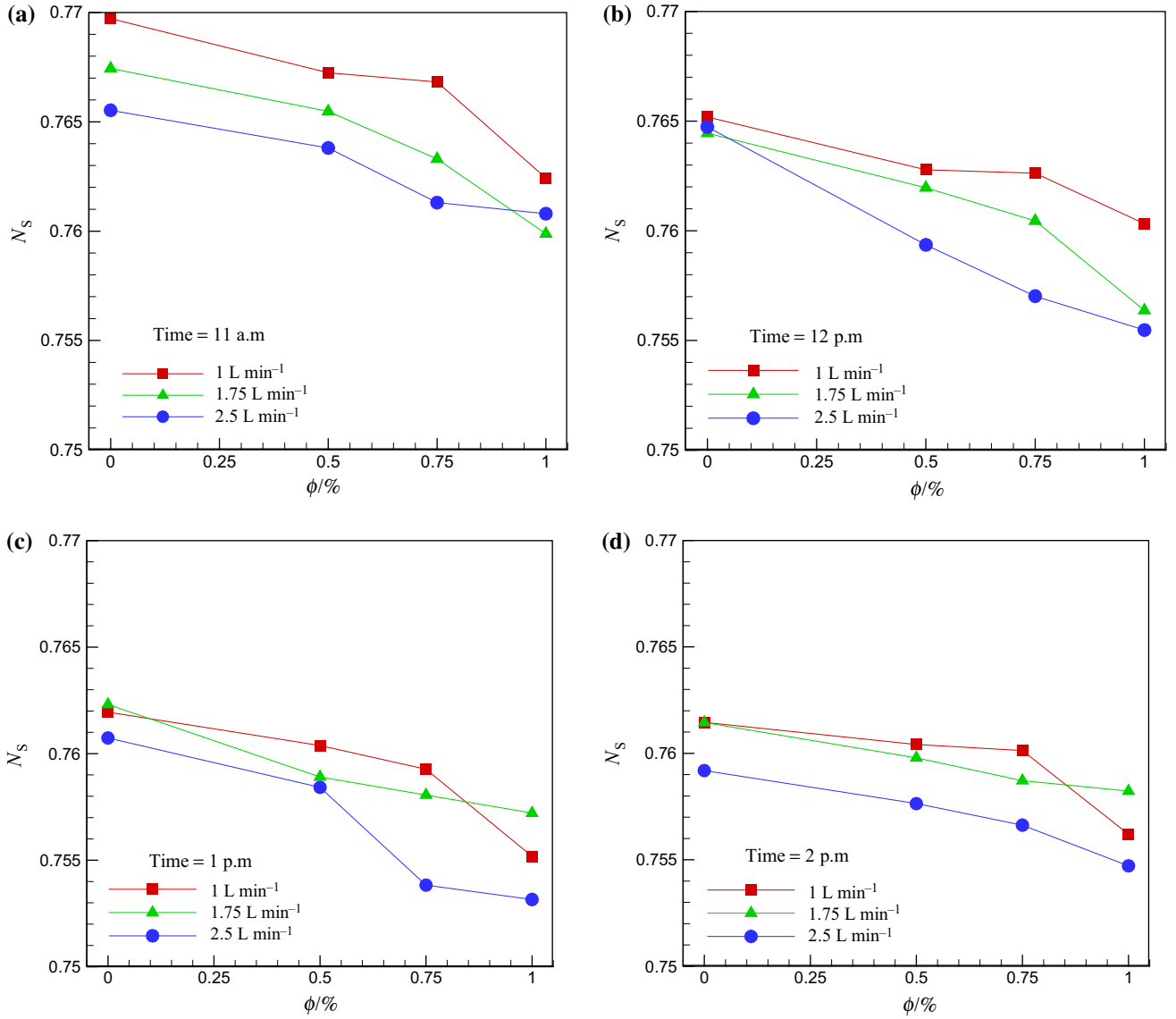

Fig. 6 Variations of entropy generation number with volume fraction for different mass flow rates and times of day

Density:

$$\rho_{nf} = \rho_f(1-\phi) + \rho_p\phi \tag{5}$$

Specific heat capacity:

$$C_{p,nf} = \frac{\rho_f C_{p,f}(1-\phi) + \rho_p C_{p,p}\phi}{\rho_{nf}} \tag{6}$$

The subscripts of f, p, and nf stand for base fluid, particle, and nanofluid, respectively. The variations of heat capacity and density for volume fractions of 0–1 % are shown in Fig. 4. As seen, with increasing the nanofluid concentration, the density increases linearly, while the heat capacity decreases nonlinearly.

Since the experiments for different volume fractions and mass flow rates have been done in different days (different weather conditions), so it is not reasonable to compare the entropy generation rate in different weather conditions with each other. To resolve this problem, a dimensionless entropy generation number (N_s) could be introduced as follows:

$$N_S = \frac{\dot{S}_{gen} T_a}{G_t A_c} \tag{7}$$

The Bejan number that shows the ratio of irreversibility due to heat transfer to the total irreversibility is written as:

$$\mathrm{Be} = \frac{\dot{S}_{gen})_H}{\dot{S}_{gen}} \tag{8}$$

in the above, $\dot{S}_{gen})_H$ includes three terms that is indicated in Eq. (1).

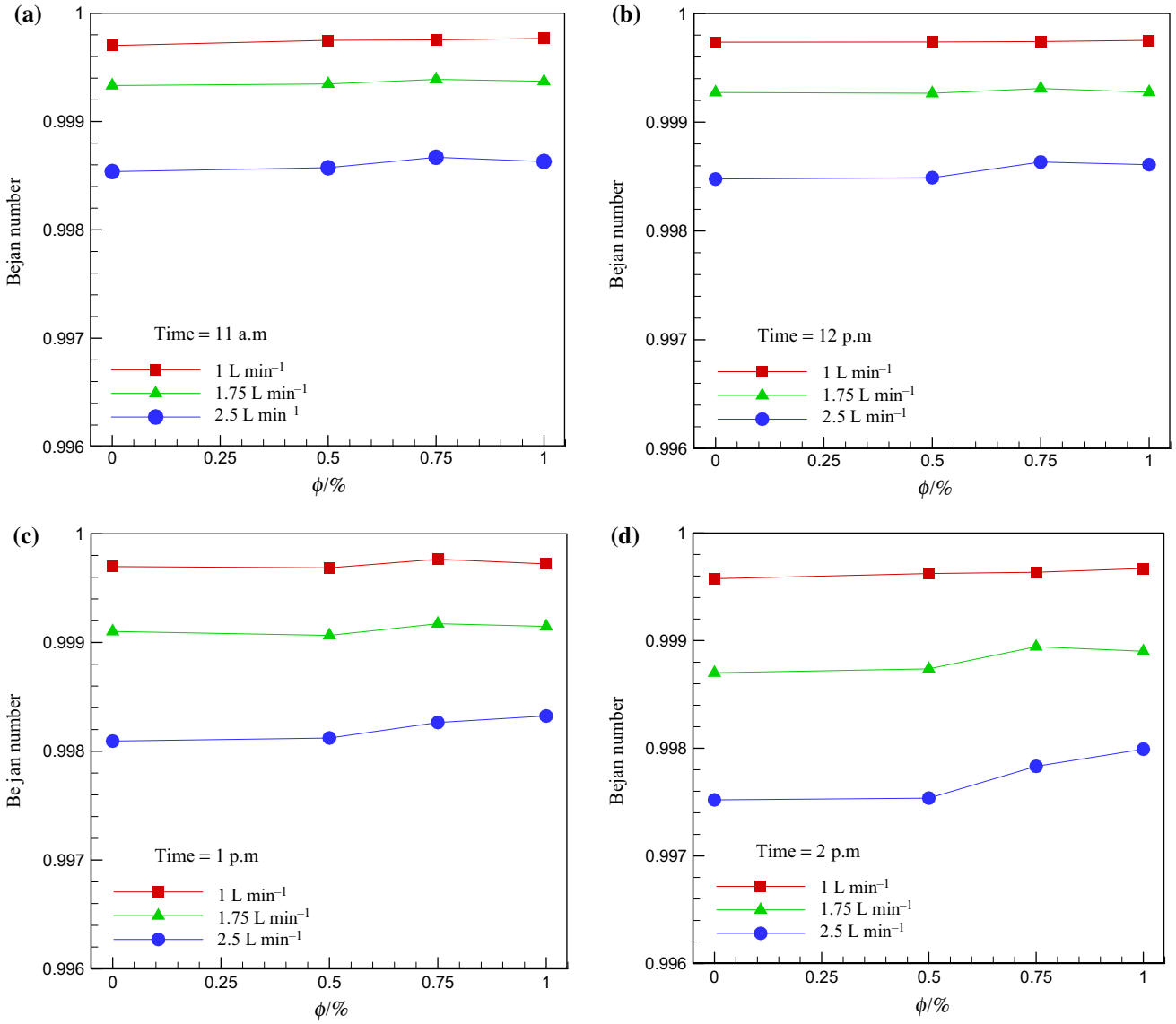

Fig. 7 Variations of Bejan number with volume fraction for different mass flow rates and times of day

Finally, the energy efficiency of the solar collector is obtained by:

$$\eta_{II} = \frac{\dot{m}\left[C_{p,nf}\left(T_{out} - T_{in} - T_a \ln\left(\frac{T_{out}}{T_{in}}\right)\right) - \frac{\Delta P}{\rho_{nf}}\right]}{G_t A_c\left(1 - \frac{T_a}{T_s}\right)} \quad (9)$$

To use the above equations, semi-steady-state conditions have been considered.

Results and discussion

The results of this study are presented in terms of exergy efficiency, dimensionless entropy generation number, and Bejan number for different volume fraction and mass flow rates. Figure 5 illustrates the variations of exergy efficiency with volume fraction for different mass flow rates. It is found that with rising nanofluid concentration from 0 to 1 %, exergy efficiency enhances by 62.7 % for a mass flow rate of 1 L min^{-1}, whereas the corresponding increases in mass flow rates of 1.75 and 2.5 L min^{-1} are 45.2 and 39.7 %, respectively. In general, it is seen that the exergy efficiency is highest for the maximum mass flow rate, i.e., 2.5 L min^{-1}. For volume fractions greater than 0.5 %, it is observed that the exergy efficiency associated with the mass flow rate of 1 L min^{-1} is higher than a mass flow rate of 1.75 L min^{-1}. Referring Eq. (9), it is found that exergy efficiency is a function of mass flow rate, pressure drop, heat capacity, and density. The interaction of these parameters determines the exergy efficiency.

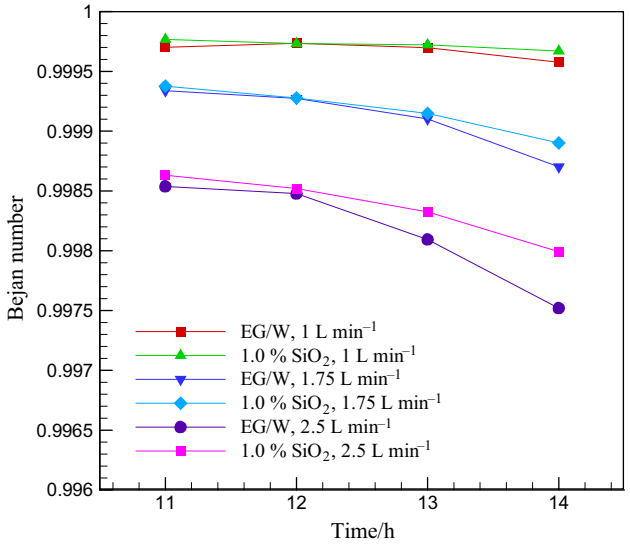

Fig. 8 Variations of Bejan number with time for different volume fractions and mass flow rates

Figure 6 presents the variations of entropy generation number with volume fraction for different mass flow rates and various times of day that correspond with different solar radiation intensities. The figure unveils that in general the entropy generation number is lowest for the mass flow rate of 2.5 L min^{-1} and is highest for the mass flow rate of 1 L min^{-1}. Also, the results elucidate that with increasing the volume fraction of nanoparticles, the entropy generation number reduces continuously. The calculations show that the pressure drop has the minimum contribution to the entropy generation in Eq. (1). The length of risers is not so long (just about 1.7 m), and on the other hand, the mass flow rates are low so that the flow in the risers is laminar. Therefore, the pressure drop magnitude that mainly depends on mass flow rate and tube dimensions will be small, and hence, its effect on entropy generation is negligible. The first term on the right-hand side of Eq. (1) has the maximum contribution (more than 90 %) to entropy generation, and also, T_S is considered to be 4350 K; therefore, the term "$\frac{1}{T_S}$" is negligible; so Eq. (1) can be reduced as:

$$\dot{S}_{gen} \approx \frac{\eta_o G_t A_c}{T_p} \tag{10}$$

Moreover, based on the definition of entropy generation number (N_S) in Eq. (7) and considering Eq. (2), one can reach the following statement:

$$N_S = \text{function}\ (T_{in}, \dot{m}\ ,\ C_{p,nf}, T_{out}, F_R U_L) \tag{11}$$

As seen, many parameters affect the value of N_S, and the interaction of these parameters determines the final value of entropy generation number.

Figure 6 also reveals that the maximum reduction in entropy generation number occurs at 12 p.m. and for 2.5 L min^{-1}. When the volume fraction increases from 0 to 1 %, the entropy generation number decreases about 1.2 %. In the previous work [28], it was concluded that nanofluids with volume fractions of 0.75 and 1 % provide nearly the same enhancements in the energy efficiency of the solar collector, but by considering the preparation cost, it was suggested to use a volume concentration of 0.75 %. In the present investigation, since the values of N_s at volume fractions of 0.75 and 1 % are very close (with <1 % difference), the volume fraction of 0.75 % may be the optimum concentration for using in the solar collector if the price of nanoparticles is involved. It should be noted a more comprehensive study is needed to select the exact optimum concentration where energy efficiency, entropy generation magnitude, and preparation costs are involved in the analysis.

Figure 7 displays the variations of Bejan number with volume fraction for different mass flow rates and times of the day. It is seen that in a given mass flow rate, the Bejan number augments with increasing the volume fraction; this implies that by particle loading, the contribution of heat transfer to total entropy generation increases. The increment of Bejan number with particle loading is more noticeable for higher mass flow rates. At a specific nanofluid concentration, it is also found that the Bejan number diminishes with increasing the mass flow rate; this means that the contribution of heat transfer to total irreversibility decreases with increasing the velocity of nanofluids in the solar collector.

Figure 8 is plotted to show the variations of Bejan number with time for different volume fractions and mass flow rates. It is observed that as time passes, the Bejan number reduces, and the decline is more visible at high mass flow rates. With passing the time, especially after 12 p.m., the inlet and absorber plate temperatures increase, and on the other hand, the solar irradiation decreases; therefore, the entropy generation due to heat transfer and consequently the Bejan number fall.

Conclusions

A theoretical study based on experimental data was performed to evaluate the second law of thermodynamics for a flat-plate solar collector where SiO_2/EG–water nanofluids with volume fractions up to 1 % were exploited. A new dimensionless entropy generation number was introduced to assess the irreversibility magnitude in the solar collector, i.e., a function of solar radiation and ambient temperature. The analysis was done for three different mass flow rates and different times of the day. The main findings of the study are summarized as follows:

- With nanoparticle loading, the exergy efficiency of solar collector enhances. The amount of increase in the

exergy efficiency depends on mass flow rate. A lower mass flow rate results in a higher augmentation in exergy efficiency.

- When nanofluid concentration changes from 0 to 1 %, exergy efficiency enhances by 62.7 % for a mass flow rate of 1 L min^{-1}, while for a mass flow rate of 2.5 L min^{-1}, the exergy efficiency ameliorates about 40 %.
- The entropy generation number decreases with increasing the nanofluid concentration.
- The entropy generation number is lowest for the mass flow rate of 2.5 L min^{-1}.
- Bejan number rises with adding nanoparticles to the base liquid. The increase highlights high mass flow rates.
- Bejan number reduces when time passes, especially after 12 p.m. when the solar radiation intensity reduces.
- The volume concentration of 0.75 % may be the optimum concentration where energy efficiency, entropy generation, and cost of nanoparticles have been considered.

Acknowledgements The authors would like to acknowledge the financial supports provided by Ferdowsi University of Mashhad under Grant No. 40342. Also, the fourth author would like to thank the "Research Chair Grant" National Science and Technology Development Agency, the Thailand Research fund (TRF), and the National Research University Project for the support.

References

1. Esfe MH, Saedodin S. Turbulent forced convection heat transfer and thermophysical properties of Mgo–water nanofluid with consideration of different nanoparticles diameter, an empirical study. J Therm Anal Calorim. 2015;119(2):1205–13.
2. Ahammed N, Asirvatham LG, Wongwises S. Effect of volume concentration and temperature on viscosity and surface tension of graphene–water nanofluid for heat transfer applications. J Therm Anal Calorim. 2016;123(2):1399–409.
3. Esfe MH, Saedodin S, Bahiraei M, Toghraie D, Mahian O, Wongwises S. Thermal conductivity modeling of MgO/EG nanofluids using experimental data and artificial neural network. J Therm Anal Calorim. 2014;118(1):287–94.
4. Bashirnezhad K, Rashidi MM, Yang Z, Bazri S, Yan WM. A comprehensive review of last experimental studies on thermal conductivity of nanofluids. J Therm Anal Calorim. 2015;122(2):863–84.
5. Esfe MH, Saedodin S, Wongwises S, Toghraie D. An experimental study on the effect of diameter on thermal conductivity and dynamic viscosity of Fe/water nanofluids. J Therm Anal Calorim. 2015;119(3):1817–24.
6. Abbasi S, Zebarjad SM, Baghban SHN, Youssefi A, Ekrami-Kakhki MS. Experimental investigation of the rheological behavior and viscosity of decorated multi-walled carbon nanotubes with TiO_2 nanoparticles/water nanofluids. J Therm Anal Calorim. 2016;123(1):81–9.
7. Esfe MH, Saedodin S, Yan WM, Afrand M, Sina N. Study on thermal conductivity of water-based nanofluids with hybrid suspensions of CNTs/Al_2O_3 nanoparticles. J Therm Anal Calorim. 2016;124(1):455–60.
8. Esfe MH, Saedodin S, Mahian O, Wongwises S. Thermal conductivity of Al_2O_3/water nanofluids, measurement, correlation, sensitivity analysis, and comparisons with literature reports. J Therm Anal Calorim. 2014;117(2):675–81.
9. Bigdeli MB, Fasano M, Cardellini A, Chiavazzo E, Asinari P. A review on the heat and mass transfer phenomena in nanofluid coolants with special focus on automotive applications. Renew Sustain Energy Rev. 2016;60:1615–33.
10. Nitiapiruk P, Mahian O, Dalkilic AS, Wongwises S. Performance characteristics of a microchannel heat sink using TiO_2/water nanofluid and different thermophysical models. Int Commun Heat Mass Transf. 2013;47:98–104.
11. Halelfadl S, Estellé P, Maré T. Heat transfer properties of aqueous carbon nanotubes nanofluids in coaxial heat exchanger under laminar regime. Exp Thermal Fluid Sci. 2014;55:174–80.
12. Maré T, Halelfadl S, Sow O, Estellé P, Duret S, Bazantay F. Comparison of the thermal performances of two nanofluids at low temperature in a plate heat exchanger. Exp Thermal Fluid Sci. 2011;35:1535–43.
13. Esfe MH, Saedodin S, Mahian O, Wongwises S. Heat transfer characteristics and pressure drop of COOH-functionalized DWCNTs/water nanofluid in turbulent flow at low concentrations. Int J Heat Mass Transf. 2014;73:186–94.
14. Esfe MH, Saedodin S, Mahian O, Wongwises S. Thermophysical properties, heat transfer and pressure drop of COOH-functionalized multi walled carbon nanotubes/water nanofluids. Int Commun Heat Mass Transf. 2014;58:176–83.
15. Mahian O, Kianifar A, Kalogirou SA, Pop I, Wongwises S. A review of the applications of nanofluids in solar energy. Int J Heat Mass Transf. 2013;57(2):582–94.
16. Kasaeian A, Eshghi AT, Sameti M. A review on the applications of nanofluids in solar energy systems. Renew Sustain Energy Rev. 2015;43:584–98.
17. Alim MA, Saidur R, Khairul MA, Rahim NA, Abdin Z. Performance analysis of a solar collector using nanofluids. Adv Mater Res. 2014;832:107–12.
18. Faizal M, Saidur R, Mekhilef S, Hepbasli A, Mahbubul IM. Energy, economic, and environmental analysis of a flat-plate solar collector operated with SiO_2 nanofluid. Clean Technol Environ Policy. 2015;17(6):1457–73.
19. Said Z, Saidur R, Rahim NA, Alim MA. Analyses of exergy efficiency and pumping power for a conventionalflat plate solar collector using SWCNTs based nanofluid. Energy Build. 2014;78:1–9.
20. Mahian O, Kianifar A, Sahin AZ, Wongwises S. Entropy generation during Al_2O_3/water nanofluid flow in a solar collector: effects of tube roughness, nanoparticle size, and different thermophysical models. Int J Heat Mass Transf. 2014;78:64–75.
21. Mahian O, Kianifar A, Heris SZ, Wongwises S. First and second laws analysis of a minichannel-based solar collector using boehmite alumina nanofluids: effects of nanoparticle shape and tube materials. Int J Heat Mass Transf. 2014;78:1166–76.
22. Mahian O, Kianifar A, Sahin AZ, Wongwises S. Heat transfer, pressure drop, and entropy generation in a solar collector using SiO_2/water nanofluids: effects of nanoparticle size and pH. J Heat Transf. 2015;137:061011–9.
23. Mahian O, Kianifar A, Sahin AZ, Wongwises S. Performance analysis of a minichannel-based solar collector using different nanofluids. Energy Convers Manag. 2014;88:129–38.
24. Said Z, Saidur R, Sabiha MA, Hepbasli A, Rahim NA. Energy and exergy efficiency of a flat plate solar collector using pH treated Al_2O_3 nanofluid. J Clean Prod. 2016;112:3915–26.
25. Said Z, Saidur R, Sabiha MA, Rahim NA, Anisur MR. Thermophysical properties of single wall carbon nanotubes and its effect on exergy efficiency of a flat plate solar collector. Sol Energy. 2015;115:757–69.

26. Shojaeizadeh E, Veysi F, Kamandi A. Exergy efficiency investigation and optimization of an Al_2O_3–water nanofluid based flat-plate solar collector. Energy Build. 2015;101:12–23.
27. Shojaeizadeh E, Veysi F. Development of a correlation for parameter controlling using exergy efficiency optimization of an Al_2O_3/water nanofluid based flat-plate solar collector. Appl Therm Eng. 2016;98:1116–29.
28. Meibodi SS, Kianifar A, Niazmand H, Mahian O, Wongwises S. Experimental investigation on the thermal efficiency and performance characteristics of a flat plate solar collector using SiO_2/EG–water nanofluids. Int Commun Heat Mass Transfer. 2015;65:71–5.
29. Bejan A, Keary DW, Kreith F. Second law analysis and synthesis of solar collector Systems. J Solar Energy Eng. 1981;103:23–8.
30. Farahat S, Sarhaddi F, Ajam H. Exergetic optimization of flat plate solar collectors. Renew Energy. 2009;34:1169–74.
31. Mahian O, Kianifar A, Kleinstreuer C, Al-Nimr MA, Pop I, Sahin AZ, Wongwises S. A review of entropy generation in nanofluid flow. Int J Heat Mass Transf. 2013;65:514–32.